## REFERENCES AND NOTES


1. A. Streitwieser Jr. and J. T. Swanson, *J. Am. Chem. Soc.* **105**, 2502 (1983); A. Streitwieser Jr., *Acc. Chem. Res.* **17**, 353 (1984); D. Wilhelm *et al.*, *J. Organomet. Chem.* **280**, C6 (1985); J. J. Stezowski *et al.*, *Chem. Commun.* **1985**, 1263 (1985); Y. Cohen *et al.*, *ibid.* **1986**, 1071 (1986); A. Sygula *et al.*, *J. Am. Chem. Soc.* **109**, 6602 (1987); J. W. Bausch *et al.*, *ibid.* **111**, 3633 (1989); B. Wind *et al.*, *J. Org. Chem.* **56**, 618 (1991); I. Sethson *et al.*, *J. Am. Chem. Soc.* **114**, 953 (1992); and references therein.
2. L. A. Paquette *et al.*, *J. Am. Chem. Soc.* **112**, 8776 (1990); W. Bauer *et al.*, *ibid.* **113**, 7093 (1991); M. Eiermann and K. Hafner, *ibid.* **114**, 135 (1992); and references therein.
3. G. Fraenkel and M. P. Hallden-Abberton, *ibid.* **103**, 5657 (1981); L. M. Jackman *et al.*, *ibid.* **109**, 6524 (1987); A. S. Galiano-Roth and D. B. Collum, *ibid.* **110**, 3546 (1988).
4. Dilithium semibullvalenide exists as a mixture of diastereomeric dimers in solution [M. J. Goldstein, T. T. Wenzel, G. Whittaker, S. F. Yates, *J. Am. Chem. Soc.* **104**, 2669 (1982); M. J. Goldstein and T. T. Wenzel, *Chem. Commun.* **1984**, 1655 (1984)].
5. In the solid state, one example of a species with two lithium ions sandwiched between two hydrocarbon monoanions has been reported [D. Bladauski, H. Dietrich, H.-J. Hecht, D. Rewicki, *Angew. Chem.* **89**, 490 (1977); *Angew. Chem. Int. Ed. Engl.* **16**, 474 (1977); D. Bladauski *et al.*, *Chem. Ber.* **112**, 1380 (1979)].
6. W. E. Barth and R. G. Lawton, *J. Am. Chem. Soc.* **88**, 380 (1966); W. E. Barth and R. G. Lawton, *ibid.* **93**, 1730 (1971).
7. L. T. Scott *et al.*, *ibid.* **113**, 7082 (1991).
8. A. Borchardt, A. Fuchicello, K. V. Kilway, K. K. Baldridge, J. S. Siegel, *ibid.* **114**, 1921 (1992).
9. J. C. Hanson and C. E. Nordman, *Acta Crystallogr. B* **32**, 1147 (1976).
10. A. Ayalon, M. Rabinovitz, P.-C. Cheng, L. T. Scott, *Angew. Chem.* **104**, 1691 (1992); *Angew. Chem. Int. Ed. Engl.* **31**, 1636 (1992); P. W. Rabideau *et al.*, *Tetrahedron Lett.* **34**, 6351 (1993).
11. The NMR data of compounds **1**, **2**, and **3** and their tetraanions in THF-$d_8$. The $^1$H and $^{13}$C data are in parts per million downfield from TMS, and the $^7$Li data are in parts per million downfield relative to LiBr (0.01M LiBr in THF as external reference). The $^1$H and $^{13}$C spectra were recorded on a Bruker AMX-400 spectrometer with a $^2$H lock. The THF-$d_7$ low-field proton band was used for calibration of $^1$H spectra (δ 3.67); the THF-$d_8$ $^{13}$C low-field signal served for calibration of the $^{13}$C spectra (δ 67.7). For anionic species, $^1$H chemical shifts varied as much as ±0.03 ppm from one sample to the next. Abbreviations: (s) singlet, (d) doublet, (m) multiplet, and (AB) AB quartet. Compound **1**: $^1$H: 7.93 (s); $^{13}$C: 127.9, 132.3, 136.9. Compound **1**$^{4-}$: $^1$H: 6.98 (s); $^{13}$C: 86.8, 95.1, 112.4; $^7$Li (210 K): −4.5 (4 Li), −11.7 (4 Li). Compound **2**: $^1$H: 8.40 (d, 1 H), 7.95 to 7.86 (m, 8 H); 1.80 (s, 9 H); $^{13}$C: 33.4, 38.1, 123.4, 127.0, 127.7, 127.8, 128.0, 128.1, 128.14 (2 C), 129.0, 130.5, 131.5, 132.0, 132.2 (2 C), 135.6, 136.5, 136.7, 137.1, 137.3, 151.3. Compound **2**$^{4-}$: $^1$H: 2.4 (s, 9 H), [6.77 (d), 6.77 (d), 7.78 (d), 7.79 (d), 6.81 (d), 6.83 (d), 6.84 (d), 6.86 (d)] (4 H), 6.89 (d, 1 H), [7.01 (d), 7.02 (d)] (1 H), [7.04 (d), 7.05 (d)] (1 H), [7.29 (d), 7.31 (d)] (1 H), [7.33 (s), 7.34 (s)] (1 H); $^{13}$C: 33.13, 33.15, 39.15 (2 C), 83.79 (2 C), 84.60, 84.73, 84.92, 85.08, 85.16, 85.27, 86.86, 86.87, 88.34 (2 C), 88.56, 88.91, 89.88, 89.89, 93.02, 93.12, 94.25, 94.31, 94.36, 94.51, 95.56, 95.68, 95.78, 95.84, 96.90, 96.94, 108.08, 108.09, 112.24 (2 C), 112.38 (2 C), 112.47, 112.53, 112.82 (2 C), 112.91 (2 C); $^7$Li (210 K): −5.0 (4 Li), −11.7 (4 Li). Compound **3**: $^1$H (190 K): 1.41 (d, 3 H), 1.77 (d, 3 H), 3.95 (m, 1 H), 7.89 (d, 1 H), 7.95 to 8.06 (m, 7 H), 8.22 (d, 1 H); $^1$H (295 K): 1.61 (d, 6 H), 3.91 (m, 1 H), 7.80 (s, 1 H), 7.87 to 7.97 (m, 7 H), 8.14 (d, 1 H); $^{13}$C (297 K): 24.8, 31.5, 122.8, 125.9, 127.7, 127.9, 128.1 (overlapping peaks), 131.2, 131.7, 131.9, 132.3, 132.8, 135.8, 136.9, 137.1, 137.4, 149.2. Compound **3**$^{4-}$: $^1$H (230 K): 1.58 (d, 3 H), 1.63 (d, 3 H), 2.5 (d, 6 H), 4.56 (broad, 2 H), [6.88 (d), (6.89, 7.08) (AB), (6.91, 6.71) (AB), 6.70 (d)] (6 H), [6.84 (d), 6.86 (d)] (2 H), [6.89 (d), 6.91 (d)] (2 H), [6.97 (d), 6.99 (d)] (2 H), [(7.06, 7.075) (AB), (7.07, 7.09) (AB), 7.095 (s), 7.10 (s)] (6 H); $^{13}$C (297 K): 25.4, 26.1, 35.0, 35.1, 84.0, 84.5, 84.9, 85.0, 86.1, 86.3, 86.4, 88.3, 88.8, 88.9, 90.0, 94.5, 95.0, 96.0, 96.2, 108.8, 111.4, 111.7, 111.8, 113.1, 113.4; $^7$Li (210 K): −3.3 (4 Li), −11.7 (4 Li).
12. P.-C. Cheng, thesis, University of Nevada, Reno (1992).
13. For a description of the general procedure for preparing such polyanions, see L. Zelikovich, R. E. Hoffman, A. Ayalon, M. Rabinovitz, *J. Chem. Soc. Perkin Trans. 2*, **1992**, 1785 (1992). The THF-$d_8$ was dried over sodium potassium alloy and vacuum transferred into the NMR tube.
14. Isopropylcorannulene was prepared by the nickel-mediated coupling of bromocorannulene (*7*) with isopropylmagnesium chloride according to the method of Kumada [K. Tamao *et al.*, *Bull. Chem. Soc. Jpn.* **49**, 1958 (1976); K. Tamao *et al.*, *Tetrahedron* **38**, 3347 (1982)].
15. M. M. Exner *et al.*, *J. Am. Chem. Soc.* **95**, 7009 (1973); P. Jutzi *et al.*, *Chem. Ber.* **122**, 1449 (1989).
16. M. J. S. Dewar and W. Thiel, *J. Am. Chem. Soc.* **99**, 4899 (1977). Lithium parameterization was taken from MNDOC [W. Thiel, *Quantum Chemistry Program Exchange* (Indiana University, Bloomington, IN, 1982), vol. 2, no. 438, p. 63.
17. The barrier for bowl-to-bowl inversion of a neutral corannulene derivative was determined to be 10.2 kcal/mol [L. T. Scott, M. M. Hashemi, M. S. Bratcher, *J. Am. Chem. Soc.* **114**, 1920 (1992)].


18. The authors thank R. S. Sheridan for stimulating discussions. Financial support for this work from the U.S.-Israel Binational Science Foundation, the U.S. Department of Energy, and the U.S. National Science Foundation is gratefully acknowledged.

11 March 1994; accepted 3 June 1994


# Electromagnetic Heating in the Early Solar Nebula and the Formation of Chondrules


Don D. Eisenhour,* Tyrone L. Daulton, Peter R. Buseck



**Certain opaque inclusions within primitive meteorites exhibit textures that suggest chondrules formed during intense, short-duration radiative heating episodes in the early solar system. Experimental support for this interpretation is provided by the textures produced when chondrule-like assemblages are heated with visible laser light. Computer simulations of radiative heating provide additional evidence for the role of electromagnetic energy in heating nebular solids by offering an explanation for the size distributions of chondrules and the presence of dusty chondrule rims. Nebular lightning and magnetic reconnection flares are possible sources of electromagnetic energy for these transient heating events.**


Chondrites, which account for ~85% of the meteorites that fall to Earth, are characterized by the presence of chondrules, millimeter-sized silicate-rich objects whose textures and spherical shapes suggest that they cooled rapidly from molten droplets floating freely in space (*1–3*). A growing body of evidence suggests that chondrules formed within the solar nebula from preexisting aggregates of dust (*2*). However, a consensus is lacking as to what was responsible for melting these aggregates, leaving an important gap in our knowledge of the processes at work during the earliest stages of the solar system's formation. Current theories include frictional heating of dust during infall into the solar nebula (*4, 5*), radiative heating during a T-Tauri phase of the sun (*6*), and heating through collisions with energetic particles produced in electrostatic discharges (lightning) (*7–10*) or magnetic reconnection flares (*10–12*). In this report, textural evidence within chondrules is described that suggests visible and near-infrared radiation played an important role in chondrule formation. Computer simulations demonstrate how the size distributions of chondrules and dusty chondrule rims can be explained as products of radiative heating.

Chondrules mainly consist of olivine [$(Mg,Fe)_2SiO_4$] and pyroxene [$(Mg,Fe)SiO_3$], which absorb little energy in the visible and near-infrared region of the electromagnetic (EM) spectrum (~0.4 to 10 μm). In contrast, opaque inclusions of troilite (FeS), pentlandite [$(Ni,Fe)_9S_8$], magnetite ($Fe_3O_4$), and Ni-, Fe-rich metal within chondrules readily absorb energy in this frequency range. The opaque minerals in some chondrules occur as unique, fluffy assemblages (Fig. 1A). These fluffy opaque inclusions (FOIs) are typically ~10 to 50 μm in diameter and consist of clusters of individual troilite or pentlandite grains with interstitial olivine or pyroxene. Rarer examples include magnetite or Ni-, Fe-rich metal as the opaque phase. Compositionally, FOIs are nearly identical to compact opaque mineral inclusions within chondrules (Fig. 1B). They differ only in that the enclosing silicate in FOIs is also intimately intermixed with the opaque phase, rather than simply surrounding it (*13*).


D. D. Eisenhour, Department of Geology, Box 871404, Arizona State University, Tempe, AZ 85287, USA.
T. L. Daulton, Department of Geology, Box 871404, and Department of Physics, Box 871504, Arizona State University, Tempe, AZ 85287, USA.
P. R. Buseck, Department of Geology, Box 871404, and Department of Chemistry, Box 871604, Arizona State University, Tempe, AZ 85287, USA.

*To whom correspondence should be addressed.

Heating chondrule-like assemblages with a visible-wavelength laser produces objects remarkably similar to natural FOIs. Olivine- and pyroxene-rich assemblages (*14*) containing compact inclusions of troilite, pentlandite, and Ni-, Fe-rich metal (Fig. 1B) were placed in an argon atmosphere and irradiated with a 10-W argon-ion laser. We varied the incident flux at the sample from $10^5$ to $10^8$ W $m^{-2}$ by defocusing the beam and varied the exposure times from 0.01 to 300 s by altering the translation rate of the sample. Two visible wavelengths (488 and 514 nm) were used to induce heating.

Textures similar to those exhibited by FOIs in chondrules were produced (Fig. 1C) for exposure times of 5 to 300 s at fluxes between $10^6$ and $10^7$ W $m^{-2}$ (*15*). FOIs were produced when the incident flux was sufficient to produce localized melt pockets around opaque inclusions. When cooled, these pockets of immiscible silicate + opaque melt failed to produce single compact opaque inclusions, but instead formed dispersed opaque assemblages that were chemically similar to, but texturally distinct from, the initial assemblages. The resemblance between naturally occurring and experimentally produced FOIs suggests that radiative heating may have been important in chondrule formation.

To model chondrule formation by radiative heating, we used the absorption properties of olivine to approximate the mean characteristics of chondrules and prechondrule aggregates; all chondrules and aggregates were assumed to be compact and spherical. These assumptions are well suited to chondrules, individual grains, and compact grain aggregates containing relatively few opaque mineral inclusions. Fluffy aggregates and objects rich in opaque minerals can be evaluated by considering deviations from these ideal objects. Planck mean absorption cross sections $Q(a,T)$ were used to express the radiative absorption and emission efficiencies of grains as a function of radius $a$ and temperature $T$ (Fig. 2). Calculations of $Q(a,T)$ were performed according to the data and procedures outlined in (*16*).

The thermal histories of grains were determined from values of $Q(a,T)$ by assuming a blackbody spectral distribution for the radiation responsible for heating (*17*). A log-normal pulse shape was used to represent the radiation's blackbody temperature as a function of time $t$, and grains were assumed to radiate into an isothermal background. A pulse duration of $10^4$ s was chosen on the basis of experimentally determined chondrule cooling rates of 0.01° to 1°C $s^{-1}$ (*18*); $10^4$ s corresponds to a cooling rate of ~0.1°C $s^{-1}$.

The thermal evolution of grains was evaluated from the relation

$$\frac{dT_g}{dt} = \frac{3\sigma}{4a\rho C_p(T_g)}[W(r)T_*^4Q(T_*) + 4T_b^4Q(T_b) - 4T_g^4Q(T_g)] \quad (1)$$

where $\sigma$ is the Stefan-Boltzmann constant; $a$ is the grain radius; $\rho$ is the mass density of the grain; $C_p$ is the heat capacity for olivine (*19*); $T_g = T_g(t)$, $T_* = T_*(t)$, and $T_b$ are the grain, light pulse, and ambient background temperatures, respectively; $Q$ is the Planck mean absorption cross section for olivine evaluated at $T_g$, $T_*$, and $T_b$; and $W$ relates the falloff in flux to distance $r$ from the emitting source. The terms containing $Q(T_*)$ and $Q(T_b)$ represent contributions to the energy of a grain from the light pulse and ambient background radiation, respectively, and the term containing $Q(T_g)$ accounts for a grain's radiative energy loss. Radiative cooling and the absorption of background radiation are assumed to occur over the entire surface of grains, an area of $4\pi a^2$, whereas light-pulse heating is assumed to be from a plane wave and, therefore, only occurs over $\pi a^2$. Peak grain temperatures for a series of grain sizes are shown in Fig. 3 (*20*).

The maximum at ~$5 \times 10^4$ μm (Fig. 3) represents the point at which thermal inertia begins to influence peak temperatures. For grains $< 5 \times 10^4$ μm in diameter (which includes all known chondrules), radiative equilibrium is approximately maintained during heating. Consequently, peak temperatures for chondrule-sized grains can be determined by considering the asymptotic relationship of Eq. 1. Setting the quantity within square brackets in Eq. 1 to zero and evaluating at the peak pulse temperature, $T_{*,max}$, we get a peak grain temperature $T_{g,max}$ of

$$T_{g,max} = \left[\frac{W(r)T_{*,max}^4Q(T_{*,max}) + 4T_b^4Q(T_b)}{4Q(T_{g,max})}\right]^{1/4} \quad (2)$$

The ability of light to preferentially heat nebular solids provides an explanation for several features exhibited by chondrules. Prominent among these is the lower limit to chondrule sizes. Chondrule diameters vary among the major chondrite groups, with

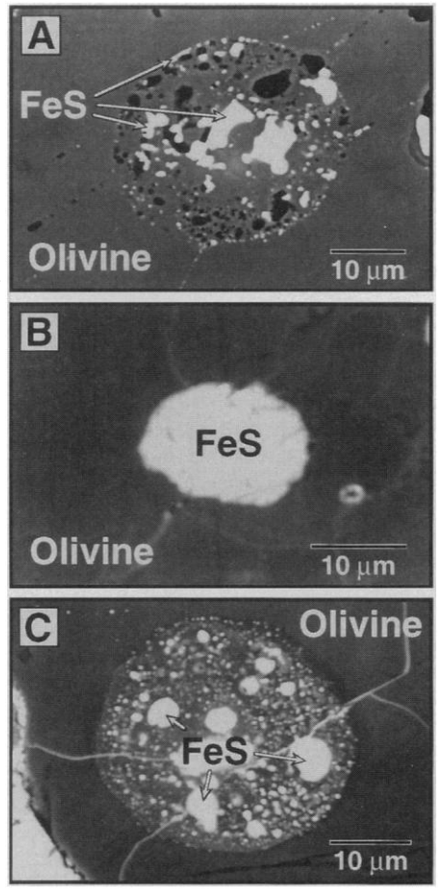


**Fig. 1.** Back-scattered electron images of (**A**) a FOI within a chondrule from the Karoonda CK4 chondrite, (**B**) a compact opaque inclusion from the Allende CV3 chondrite (typical of experimental textures before laser heating), and (**C**) a FOI produced by heating a compact opaque inclusion in situ to just above its melting point with 514-nm laser light (heating time, 30 s). Note the similarity between the natural FOI in (A) and the laser-produced FOI in (C).

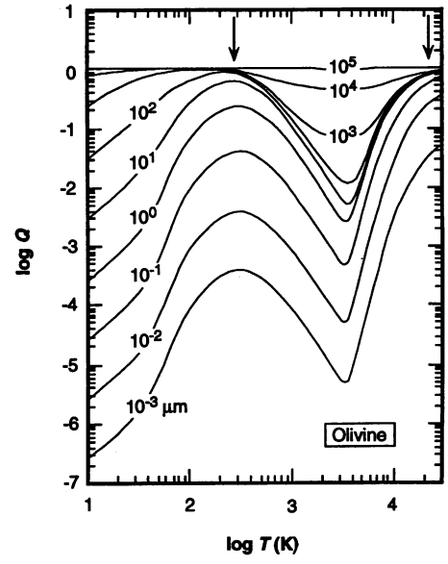


**Fig. 2.** Planck mean absorption cross sections $Q(a,T)$ for a range of olivine grain sizes. The cross sections represent the efficiency with which grains absorb or emit Planck radiation as a function of temperature relative to a perfect blackbody. The maxima at 300 K and >20,000 K (arrows) correspond to regions of strong absorption for olivine in the infrared (~10 to 33 μm) and ultraviolet (<0.4 μm) portions of the EM spectrum, respectively. The minimum at 3000 K corresponds to the transparent window of olivine between ~0.4 and 10 μm.

means ranging from ~0.15 to 1.0 mm and minima between ~0.03 and 0.25 mm (*21*). Although there is some debate as to the actual minimum chondrule size in any given chondrite, sizes do not appear to trail off to zero (*22*). The lower cutoff to chondrule sizes is demonstrated by the fact that chondrule distributions conform to a Weibull probability function with a nonzero size intercept (Fig. 4) (*23*).

It is difficult to explain the lower limit to chondrule sizes by precursor dust-aggregate distributions. Models of dust agglomeration in turbulent nebular environments typically predict an abundance of grains and grain aggregates smaller than minimum chondrule sizes (Fig. 4). Sorting has been proposed to account for chondrule size distributions (*24*), but there is little observational support for this explanation. If chondrule populations are products of sorting, then numerous meteorites containing complementary populations of smaller or larger chondrules should be observed. This is not the case. Mean chondrule sizes vary with chondrite type, but each population is chemically and isotopically distinct, precluding the possibility that all chondrules were derived from a single source.

Radiative heating provides a possible solution; small grains and aggregates existed during chondrule formation but were not melted because of their inability to absorb light efficiently. The lower size limit of ~0.2 mm implied by the peak temperatures reached by grains (Fig. 3) agrees well with observed minimum chondrule sizes. Changes in the peak pulse temperature can affect both mean and minimum chondrule diameters and may explain chondrule size variations among chondrite groups. Assuming similar initial dust distributions, raising the peak pulse temperature by 20% shifts the minimum chondrule size downward by nearly an order of magnitude.

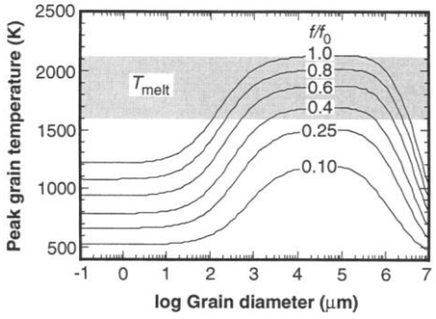


**Fig. 3.** Peak grain temperatures plotted as a function of size for heating at various distances from a light-producing source. Distances are represented in terms of falloff in flux, $f/f_o$, where $f_o$ is the radiative flux emitted at the source and $f$ is the attenuated flux at a given distance. A log-normal pulse shape was used to simulate heating, with pulse duration defined as the amount of time that the pulse temperature exceeds 1/*e* (37%) of its maximum temperature ($T_{*,max}$). In this example, the pulse duration is $10^4$ s, $T_{*,max}$ is 3000 K, and the ambient background temperature is 400 K. The shaded region ($T_{melt}$) corresponds to the range of solidus temperatures for natural chondrules.

The tail at the upper end of chondrule size distributions most likely reflects variations in initial dust-aggregate populations. From Fig. 3, it is apparent that the upper limit to chondrule sizes cannot be attributed to thermal inertia. To truncate chondrule distributions in the millimeter size range, pulse durations on the order of 30 s would be required, which is much faster than can be reconciled with chondrule cooling rates. However, agglomeration models predict a decrease in the abundance of aggregates with increasing size for chondrule-sized aggregates, just as is observed at the upper end of chondrule distributions (Fig. 4). If the upper end of chondrule distributions does reflect precursor aggregate sizes, then variations among chondrule distributions should be valuable in guiding models of dust agglomeration within regions of chondrite formation.

The formation of sintered dusty rims around chondrules (*25*) is also consistent with an environment dominated by radiative heating. Many chondrules exhibit dusty rims that are predominantly composed of silicate grains ≤10 μm in diameter. These rims commonly show evidence of heating, often to the point of melting. Apparently, dust either partially melted on contact with newly formed chondrules or was reheated after accumulation. The lack of chondrules ≤10 μm in size, despite the prevalence of dust grains ≤10 μm available for rim formation, is problematic if all solids were heated equally. However, with radiative heating, dusty-rim formation through collisions between small, cooler grains and newly formed chondrules would be a natural product of the chondrule-forming process.

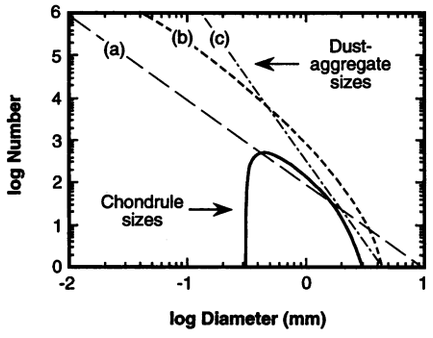


**Fig. 4.** Size distributions of chondrules and nebular dust aggregates. The chondrule curve is a Weibull function fit to chondrule data from the Bjurböle L4 chondrite (*23*). Dotted curves represent dust-aggregate distributions predicted in turbulent protoplanetary accretion disks: (a) "equilibrium" distribution at 2 astronomical units (AU) resulting from balance between coagulation and disruption (*27*); (b) distribution near the midplane at 1 AU after 10,000 years with a solids/gas ratio of ~0.4 (*28*); (c) steady-state distribution reached at the outer edge of the disk with a constant influx of small (<1 μm) grains (*29*). Note that radial distances vary considerably among these aggregation models. For direct comparison with chondrule sizes, dust-aggregate diameters have been adjusted to reflect chondrule densities.

Only chondrule-formation theories involving the sun as a heat source assume that dust was heated by EM radiation. However, nebula-wide heating out to a distance of ~3 to 5 astronomical units (the probable region of chondrule formation) during highly luminous solar events is difficult to reconcile with the localized heating implied by chondrule cooling rates. Theories involving electrostatic discharges and magnetic reconnection flares presume chondrule heating occurred primarily by collisions with energetic particles (*10–12*). Possibly, the contribution of EM energy to the heating of dust has been underestimated in these theories.

Numerical models of terrestrial lightning suggest that the majority (~70%) of the total input energy is dissipated in the form of EM radiation (*26*). A similar situation could exist for magnetic reconnection flares occurring high above the nebular midplane (*12*). Energetic particles cascading into denser regions of the nebula may dissipate energy in the form of EM radiation through the collisional ionization of neutral gas. In this case, chondrules would be heated by the light produced in intense nebular auroral displays. Additional work on the EM radiation released by magnetic and electrostatic discharges within the early solar nebula is needed to properly evaluate these processes.

## REFERENCES AND NOTES


1. R. H. Hewins, in *Meteorites and the Early Solar System*, J. F. Kerridge and M. S. Mathews, Eds. (Univ. of Arizona Press, Tucson, AZ, 1988), pp. 660–679.
2. J. N. Grossman, *ibid.*, pp. 680–696.
3. ———, A. E. Rubin, H. Nagahara, E. A. King, *ibid.*, pp. 619–659.
4. J. A. Wood, *Mem. Natl. Inst. Polar Res. Special Issue* **30**, 84 (1983).
5. ———, *Earth Planet. Sci. Lett.* **70**, 11 (1984).
6. G. H. Herbig, in *The Origin of the Solar System*, S. F. Dermott, Ed. (Wiley, New York, 1978), pp. 219–235.
7. F. L. Whipple, *Science* **153**, 54 (1966).
8. A. G. W. Cameron, *Earth Planet. Sci. Lett.* **1**, 93 (1966).
9. K. L. Rasmussen and J. T. Wasson, in *Papers Presented to the Conference on Chondrules and Their Origins* (Lunar and Planetary Institute, Houston, TX, 1982), p. 53.
10. G. Morfill, H. Spruit, E. H. Levy, in *Protostars and Planets III*, E. H. Levy and J. I. Lunine, Eds. (Univ. of Arizona Press, Tuscon, AZ, 1993), pp. 939–978.
11. C. P. Sonett, *Geophys. Res. Lett.* **6**, 677 (1979).
12. E. H. Levy and S. Araki, *Icarus* **81**, 74 (1989).
13. A total of 34 thin sections (21 different chondrites) representing nine chondrite classes (EH, H, L, LL, CV, CO, CM, CK, and CI) were surveyed for the presence of FOIs. Their abundances vary greatly both within and between chondrite classes. They are most abundant within CVs and CKs; in Allende, a

well-studied CV, they are present in >80% of the chondrules. FOIs are rare or absent in the EH, H, and L chondrites. No correlation was observed between shock grade and the presence or absence of FOIs. S. E. Haggerty and M. McMahon [*Proc. Lunar Planet. Sci. Conf.* **10**, 851 (1979)] show FOI-like textures from Allende in their figure 1, a, h, and k.
14. Powdered mixtures containing ~60 weight % San Carlos olivine, ~39 weight % Bamble enstatite, and ~1 weight % troilite, pentlandite, magnetite, and Ni-Fe metal were pressed into pellets, heated to 1560°C (just above the enstatite solidus), and then cooled at 0.1° to 0.01°C $s^{-1}$. Samples were cut into 0.5-mm-thick sections and polished.
15. The largest uncertainties in extrapolating experimentally determined fluxes to nebular conditions result from differences in the heat-transfer properties of 0.5-mm-thick plates and millimeter-sized spheres and from the possibility that chondrules may have been heated by more than one mechanism. If a secondary heat source, such as energetic particles, facilitated chondrule heating, less radiant energy may be required to form FOIs.
16. Data and procedures were followed as described by R. C. Gilman [*Astrophys. J. Suppl.* **28**, 397 (1974)], except for the condition $(2\pi a/\lambda)(n^2 + k^2)^{1/2} > 0.1$. For this case, $Q(a,T)$ was calculated according to the large-particle approximation for $K(\omega)$ given by H. C. van de Hulst [*Light Scattering by Small Particles* (Dover, New York, 1981), p. 175], which yields more realistic Planck mean absorption cross sections for grains >1 μm than the extrapolation method used by Gilman.
17. For a similar evaluation addressing the survival of dust within the radiation field associated with supernovae, see S. W. Falk and J. M. Scalo, *Astrophys. J.* **202**, 690 (1975).
18. R. H. Hewins and P. M. Radomsky, *Meteoritics* **25**, 309 (1990).
19. R. A. Robie, B. S. Hemingway, J. R. Fisher, *U. S. Geol. Surv. Bull.* **1452**, 363 (1979).
20. In estimating peak chondrule temperatures, the greatest uncertainties lie in the spherical approximation used for prechondrule aggregates and in the spectral distribution of the radiation assumed for heating. Nonblackbody spectral distributions produce comparable results if >90% of the total energy is located within the region ~0.4 to 10 μm. Additionally, above ~2300 K, molten chondrules may undergo significant evaporation, reducing their sizes and limiting their peak temperatures [A. Hashimoto, *Geochem. J.* **17**, 111 (1983)].
21. Unique examples exist where mean chondrule diameters are ~0.02 mm and minumums approach 0.001 mm, for example, chondrite ALH85085 and a microchondrule-bearing clast from Piancaldoli. See review in (*3*).
22. D. W. Hughes, *Earth Planet. Sci. Lett.* **39**, 371 (1978).
23. P. M. Martin and D. W. Hughes, *ibid.* **49**, 175 (1980).
24. R. T. Dodd, *ibid.* **30**, 281 (1976).
25. A. E. Rubin, *Geochim. Cosmochim. Acta* **48**, 1779 (1984).
26. A. H. Paxton, R. L. Gardner, L. Baker, *Phys. Fluids* **29**, 2736 (1986).
27. S. J. Weidenschilling, *Icarus* **60**, 553 (1984).
28. H. Mizuno, W. J. Markiewicz, H. J. Fölk, *Astron. Astrophys.* **195**, 183 (1988).
29. S. J. Weidenschilling and J. N. Cuzzi, in (*10*), pp. 1031–1061.
30. We thank J. W. Larimer, J. A. Tyburczy, and S. J. Weidenschilling for helpful discussions, J. Menendez and G. Wolf for use of their laser facilities, A. G. W. Cameron and an anonymous reviewer for thorough and helpful reviews, and J. C. Clark for assistance with the scanning electron microscopy and electron microprobe analysis; the electron microprobe was purchased with the aid of NSF grant EAR-840816. C. F. Lewis, C. B. Moore, and the Center for Meteorite Studies at Arizona State University are gratefully acknowledged for supplying samples. This study was supported by grant NAGW-3386 from the National Aeronautics and Space Administration.

14 March 1994; accepted 8 June 1994

# Saturation of Cubic Optical Nonlinearity in Long-Chain Polyene Oligomers

Ifor D. W. Samuel, Isabelle Ledoux, Christophe Dhenaut, Joseph Zyss,* Harold H. Fox, Richard R. Schrock, Robert J. Silbey

**The scaling of the cubic nonlinearity γ with chain length in polyenic molecules has received considerable theoretical attention. Earlier experimental investigations have been restricted to oligomers with fewer than 20 double bonds because of problems associated with the synthesis and solubility of conjugated molecules. These synthetic difficulties have been overcome in the present study by the use of modern living polymerization techniques. Solution measurements of γ as a function of chain length in long-chain (up to 240 double bonds) model polyene oligomers are reported. A saturation of the increase of γ with chain length is observed, and the onset of this saturation occurs for chain lengths considerably longer than predicted from theory.**

The study of polyenes and their oligomers is important for nonlinear optics because these materials have large third-order nonlinearities and because they are used as model conjugated systems and as building blocks for nonlinear optical molecules (*1*, *2*). The magnitude of the cubic nonlinearity γ and its scaling with the number of double bonds $N$ have received considerable theoretical attention (*3*–*18*). These theories range from simple tight-binding (or Hückel) models to fully correlated π-electron models such as that of Pariser, Parr, and Pople (PPP). For small $N$, a power-law dependence $\gamma = kN^{\alpha}$ is found to approximate the theoretical results in all models, with α between 3 and 6, depending on the model used and the calculation. For large $N$ (thermodynamic limit), γ becomes linear in $N$ and $\gamma/N$ therefore becomes constant.

This saturation is predicted to occur at different values of $N$ in different models: Models such as Hückel that do not include electron correlation tend to predict saturation at rather large $N$ (>50), whereas theoretical models that include electron correlation predict saturation at smaller $N$ (~20). Although the latter calculations are subject to large errors in the large $N$ limit as a result of the limitations of computer storage, it is generally believed that they are semiquantitative. However, the implicit assumption of these models is that the parameters in the semiempirical Hamiltonian (that is, PPP) that are valid for small molecules are also valid for large molecules. If this is not so, the calculations may be seriously in error. Experimental investigation has proved difficult as a result of difficulties with synthesis and the poor solubility of polyenic oligomers. This has restricted earlier studies to molecules with fewer than 20 double bonds, and no saturation of $\gamma/N$ has been observed thus far (*19*–*26*).

The controlled synthesis of long-chain conjugated oligomers has recently become possible as a result of progress in living polymerization techniques (*27*). We report here measurements of γ as a function of $N$ in soluble long-chain model polyene oligomers with up to 240 double bonds (see Fig. 1). We have observed a saturation of $\gamma/N$ in these very much longer polyenic systems. We synthesized the molecules by cyclopolymerization in a living manner, using a molybdenum alkylidene catalyst to give a polyenic backbone substituted with five- and six-membered rings. This procedure gives good control over the length of the resulting oligomers. Molecular weights were measured by gel permeation chromatography against polystyrene, and the polydispersity was typically 1.2, indicating a fairly narrow distribution of chain lengths. Full details of the preparation and characterization of these molecules are given elsewhere (*27*).

The third-order nonlinearity γ was measured in tetrahydrofuran (THF) solution by the Maker fringe method, and data analysis was performed as previously described (*28*). Excitation at 1.91 μm was provided by a longitudinal monomode Q-switched Nd:yttrium-aluminum-garnet

I. D. W. Samuel, I. Ledoux, C. Dhenaut, J. Zyss, France Telecom-CNET-Centre Paris B-Laboratoire de Bagneux, 196 avenue Henri Ravera, 92220 Bagneux, France.
H. H. Fox, R. R. Schrock, R. J. Silbey, Department of Chemistry, Massachusetts Institute of Technology, Cambridge, MA 02139, USA.

*To whom correspondence should be addressed.